Sensors & Actuators: B. Chemical 405 (2024) 135333

Contents lists available at ScienceDirect

Sensors and Actuators: B. Chemical

journal homepage: www.elsevier.com/locate/snb

Highly efficient persistent luminescent nanozymes-based luminescence-colorimetric dual-mode sensor for total antioxidant capacity assay

Li-Xia Yan [a,b,c,d], Zhu-Ying Yan [e], Xu Zhao [a,b,c], Li-Jian Chen [a,b,c], Xiu-Ping Yan [a,b,c,d,*]

[a] State Key Laboratory of Food Science and Resources, Jiangnan University, Wuxi 214122, China
[b] International Joint Laboratory on Food Safety, Jiangnan University, Wuxi 214122, China
[c] Institute of Analytical Food Safety, School of Food Science and Technology, Jiangnan University, Wuxi 214122, China
[d] Key Laboratory of Synthetic and Biological Colloids, Ministry of Education, Jiangnan University, Wuxi 214122, China
[e] Analysis and Testing Center, Jiangnan University, Wuxi 214122, China

ARTICLE INFO

Keywords:
Persistent luminescent nanozymes
Dual-mode sensor
Total antioxidant capacity
Afterglow luminescence
Peroxidase-like
Luminescence-colorimetric sensor

ABSTRACT

Total antioxidant capacity (TAC) is a vital parameter to assess the gross antioxidant activity in biological and food matrices. Accurate determination of TAC has become increasingly important for health monitoring and dietary guidance. Here, we report a persistent luminescent nanozyme (ZGO-Pt) based luminescence-colorimetric dual-mode sensor for selective determination of TAC. ZGO-Pt was fabricated based on $ZnGa_2O_4$:Cr nanoparticles (ZGO) with platinum nanoflower as synthetic additive. The prepared ZGO-Pt exhibited fascinating peroxidase-mimetic activity and persistent luminescence, and enabled effectively catalysis of the oxidation of colorless 3,3′,5,5′-tetramethylbenzidine (TMB) to blue oxTMB. Meanwhile, the generated oxTMB gave strong absorption at 652 nm to quench the luminescence of ZGO-Pt at 700 nm via the inner filter effect. Antioxidants could compete with the oxidable TMB or reduce oxTMB to TMB, resulting in the simultaneous variations of blue color and luminescence to provide the basis for dual-mode assay for TAC. The highly efficient catalysis of ZGO-Pt (K_m, 3.12 mM for H_2O_2, 0.592 mM for TMB) allows the dual-mode sensor to realize precise determination of TAC with a wide linear range (0.5–200 μM and 1–300 μM for colorimetric and luminescence mode, respectively) and low limit of detection (LOD, 0.05 μM and 0.78 μM for colorimetric and luminescence mode, respectively). The developed dual-mode sensor was successfully applied to the determination of TAC in vitamin tablet, beverages and fruits. This work provides an efficient persistent luminescent nanoparticle-based nanozyme for a facile TAC assay with further vision in biosensing and food technology.

1. Introduction

The increasing life stress and unhealthy living habits pose the over production of free radicals, disrupting the redox homeostasis in human body [1]. Living organisms defense can be overwhelmed by the imbalance between reactive species generation and elimination [2]. There is accumulating evidences for redox damage involved inflammatory and degenerative diseases [3,4]. Thus, additional protection is required to balance the oxidative status. Antioxidants play a major part in scavenging free radicals and effectively counteracting the oxidative stress and oxidative damage of cellular organs [5,6]. However, most antioxidants have to be supplemented from exogenous nutrition since it cannot be produced by human organisms themselves [7,8]. Antioxidants such as flavonoids, carotenoids, anthocyanidins, ascorbic acid are abundant in fruits and vegetable foods [9–11]. Besides, a wide array of antioxidants is exogenously added to foods, medicines and cosmetics. Considering that the dosage of antioxidants is closely related to their antioxidant capacity, it is of great significance to get quantitative information of antioxidants in fruits or exogenous added foods. However, individual antioxidant is difficult to determine due to its large variety and the possible interactions between the involved antioxidants. Thus, total antioxidant capacity (TAC) is adopted as an antioxidant index [12], acting a vital role in assessing high-risk diseases and providing reasonable dietary guidance for modulating oxidative stress [13]. Hence, establishing accurate methods for the determination of TAC in foods and drinks is of great clinical significance for disease prevention and

* Corresponding author at: State Key Laboratory of Food Science and Resources, Jiangnan University, Wuxi 214122, China.
E-mail address: xpyan@jiangnan.edu.cn (X.-P. Yan).

https://doi.org/10.1016/j.snb.2024.135333
Received 9 November 2023; Received in revised form 19 December 2023; Accepted 9 January 2024
Available online 12 January 2024

prognosis management.

Up to now, various analytical methods for TAC have been developed, such as colorimetry, fluorometry, chromatography, and electrochemical categories [14–17]. Among them, colorimetric method is frequently exploited due to its intrinsic advantages for fast and cost-effective naked eye detection and easy on-site analysis [18,19]. A typical mode of TAC colorimetric assay involves exploiting the competition mechanism between oxidable chromogenic substrates and antioxidants. A robust oxidation strategy is a prerequisite for obtaining excellent analytical performance in this mode. Recently, the emergence of nanozymes open up new perspectives for the design of oxidation process due to their superior stability, low manufacturing cost and robust catalytic performance [20–22]. In general, the peroxidase-mimicking nanozymes are exploited to catalyze hydrogen peroxide and implement oxidation for colorimetric determination of TAC [23,24]. However, such previous nanozymes rely on a single function of mimicking enzymes with single signal output, and its corresponding solution-based colorimetric analysis is susceptible to detection environment, apparatus, and operation [25]. Therefore, a sensing assay based on multi-signals constitutes a good ability for convenient preliminary screening and accurate diagnosis, ensuring enhanced detection sensitivity and reliability.

Fluorescence sensors have clear principles and are unaffected by the suspended solids or the color of the sample solution, showing distinct advantages in bioanalysis and food monitoring. Therefore, technologies that combine the principles of colorimetric and fluorescent methods will highlight the advantages of each technique for better adapting to various complex detection requirements to fulfill highly sensitive detection of TAC. Nevertheless, most fluorescence methods require continuous external light source excitation to produce fluorescent signal, and thus subject to interference from autofluorescence of sample matrix, which seriously affects the accuracy of the detection. Hence, it is imperative to develop a sensitive method for autofluorescence-free determination of TAC in complex samples.

Persistent luminescence nanoparticles (PLNPs) can efficiently avoid scattering light and autofluorescence interferences from complex matrices with no need for in situ excitation, enabling autofluorescence-free determination with a significantly improved signal-to-noise ratio [26–28]. However, to our knowledge, there are no applications of PLNPs in dual-signal mode of luminescence and colorimetry for sensing.

Herein, we report an NIR-emitting PLNP nanozyme as a dual-signal sensor of luminescence and colorimetry for TAC assay. The PLNP nanozyme (ZGO-Pt) was fabricated based on $ZnGa_2O_4$:Cr nanoparticles (ZGO) with Pt nanoflower as synthetic additive. The prepared ZGO-Pt not only exhibits excellent peroxide-mimicking enzyme activity, but also keeps the original NIR-emitting persistence luminescence (at 700 nm) and uniform small size (ca. 6 nm) of $ZnGa_2O_4$:Cr. The excellent peroxidase-mimetic activity of ZGO-Pt allows the oxidation of colorless 3,3′,5,5′-tetramethylbenzidine (TMB) to blue oxidized TMB (ox-TMB), laying a foundation for colorimetric detection. Meanwhile, the generated oxTMB gives strong absorption at 652 nm to quench the luminescence of ZGO-Pt, providing a huge space for “turn on” luminescence sensing. Antioxidants can compete with the oxidable chromogenic substrate or reduce the oxidized substrate back, accompanied by a concentration-dependent distinct blue discoloration and a “turn-on” luminescence recovery to allow a dual-signal mode of colorimetry and luminescence for TAC assay. Furthermore, the developed dual-mode assay was successfully applied to the determination of TAC in various samples such as vitamin C tablet, fruits and drinks. In virtue of the needless in situ excitation, autofluorescence interference free and excellent nanozyme performance of ZGO-Pt, the developed assay exhibits bright prospects in food technology and healthcare field.

2. Experimental section

2.1. Materials and chemicals

Zinc nitrate hexahydrate ($Zn(NO_3)_2{\cdot}6\ H_2O$, 99.99%), gallium nitrate ($Ga(NO_3)_3$, 99.99%), chromic nitrate ($Cr(NO_3)_3{\cdot}9\ H_2O$, 99.99%), chloroplatinic acid hexahydrate ($H_2PtCl_6{\cdot}6\ H_2O$) and pluronic (F127) were purchased from Aladdin (Shanghai, China). 3,3′,5,5′-tetramethylbenzidine (TMB), 2,2′azino-bis (3-ethylbenzthiazoline-6-sulfonic acid) (ABTS), o-phenylenediamine (OPD) were purchased from Sigma-Aldrich China (Shanghai, China). Ascorbic acid (AA) and potassium bromide (KBr) were obtained from Sinopharm Chemical Reagent Co., Ltd. (Shanghai, China). Total antioxidant capacity (TAC) assay kit (DPPH) was obtained from Maclin Biochemical Technology Co., Ltd. (Shanghai, China). Ultrapure water was obtained from Wahaha Group Co. (Hangzhou, China). Acetate buffer solution (25 mM, pH 4.0) was used as the working buffers.

2.2. Synthesis of ZGO-Pt

Platinum nanoflower was used as the synthetic additive to synthesize PLNP-Pt nanozyme. The Pt nanoflower was prepared as follows [29,30]: F127 (0.9 g) and KBr (2 g) were mixed in 20 mL of ultrapure water under ultrasound, then AA aqueous solution (35 mL, 0.1 M) was added. After 20-min ultrasonic shaking, 1.5 mL of H_2PtCl_6 aqueous solution (0.2 M) was added, and the mixture was kept at 70 °C for 12 h. The final sediment particles were collected by centrifugation (4035 g for 10 min), washed with ultrapure water twice and redispersed in ultrapure water (40 mL) for further use.

A typical one-pot hydrothermal process was used to prepare ZGO-Pt. In brief, the precursors (1 mmol Zn^{2+}, 2 mmol Ga^{3+}, 0.003 mmol Cr^{3+}) and 300 μL of above Pt nanoflower aqueous solution were mixed under vigorous stirring, then ammonium water (28%, wt) was added rapidly to the above solution and the pH value was adjusted to approximately 8 with vigorous stirring. The resulting turbid solution was stirred vigorously at room temperature for 1 h and further transferred to a Teflon-lined autoclave (reacted at 220 °C, 24 h). The as-prepared ZGO-Pt nanoparticles were collected by centrifugation and washed with ethanol.

2.3. Optimization of assay parameters

A mixture solution of TMB (1 mM), H_2O_2 (20 mM) and ZGO-Pt solution (0–300 μg mL^{-1}) in 400 μL acetate buffer (pH 3.0–8.0, 25 mM) was used for optimization. The parameters optimized included solution pH, concentration of ZGO-Pt, reaction time, reaction temperature. Assay parameters were optimized via a univariate method with the absorbance at 652 nm as the figure of merit. Three to four cycles of univariate studies were needed to adjust the fixed parameters to optimal values in each univariate study.

2.4. Steady-state kinetics study

A steady-state kinetic experiment was conducted by altering the TMB concentration (0.1–1.0 mM) with a stable concentration of H_2O_2 (40 mM), ZGO-Pt (100 μg mL^{-1}) and made up to 400 μL with acetate buffer solution (pH 4.0, 25 mM), or changing H_2O_2 concentration (1–10 mM) with a fixed TMB concentration (1 mM) and ZGO-Pt (100 μg mL^{-1}). The respective absorbance changes at 652 nm were monitored by multifunctional microplate reader. The Michaelis-Menten constant (*K*m) was calculated according to the Lineweaver-Burk Plot: $1/v = K_m/(V_{max}[S]) + 1/V_{max}$, where v represents the initial velocity, V_{max} represents the maximal reaction velocity, and [S] is the substrate (TMB or H_2O_2) concentration.

2.5. Preparation of samples

Vitamin C tablet, fresh fruits including tomato, kiwi and lemon, and vitamin C fortified type of compound drinks were collected from Taobao and a local supermarket. 15 mg of Vitamin C tablet was dissolved in 5 mL of ultrapure water. Three compound drinks were used without treatment. 11.2 g of tomato, 13.8 g of kiwi fruit and 16.2 g of lemon were mixed with 10 mL of ultrapure water, followed by juicing. The mixture was then centrifuged at 6000 g for 10 min to remove the residue. The resulting supernatants were filtered with gauze. The three fruit samples were spiked with AA standard at the final concentrations of 10 μM, 100 μM, 150 μM for recovery experiments.

2.6. Determination of AA and TAC

TMB solution (10 μL, 40 mM) and H_2O_2 solution (10 μL, 0.8 M) were mixed with ZGO-Pt solution (15 μL, 4 mg mL^{-1}) and made up to 400 μL with acetate buffer solution (pH 4.0, 25 mM). The mixture solution was reacted at 35 °C under gentle shaking for 40 min. Then, 70 μL of AA solution (or sample solution) was added to the above mixture solution. After that, the luminescence intensity at 700 nm of the solution was measured on F-7000 fluorescence spectrometer in the phosphorescence mode (excitation at 254 nm, slit widths for excitation and emission, 10 nm), and the absorbance (652 nm) of the solution was recorded by multifunctional microplate reader.

3. Results and discussion

3.1. Fabrication and characterization of ZGO-Pt nanozymes

Scheme 1 shows the fabrication of ZGO-Pt and its application for luminescence-colorimetric dual-mode sensing of TAC. Platinum nanoflower was used as synthetic additive to synthesize PLNP-Pt nanozyme via a typical one-pot hydrothermal method. The as-synthesized ZGO-Pt integrates the merit of autofluorescence-free persistent luminescence (PL) sensor of PLNP and excellent peroxide-mimicking enzyme activity of nanozymes. The good peroxidase-mimetic activity of ZGO-Pt allows the oxidation of TMB to blue oxTMB, meanwhile, the generated oxTMB gives strong absorption at 652 nm to quench the luminescence of ZGO-Pt. Antioxidants will compete with the oxidable TMB or reduce the oxidized oxTMB to TMB, accompanied by a concentration-dependent distinct blue discoloration and a turn-on luminescence recovery, allowing us to develop a dual-signal mode of colorimetric and luminescence sensor for TAC.

Pt nanoflower prepared using F127 as the structure-directing agent was spherical with a uniform size and a diameter of ~70 nm (Fig. 1A). Interestingly, the prepared ZGO-Pt with Pt nanoflower as synthetic additive was granular with the diameter of 5.6 ± 1.0 nm (Fig. 1B,C). ZGO-Pt possess typical granular morphology and sub-10 nm size as ZGO PLNPs (Fig. S1), indicating that the addition of Pt nanoflower in the synthesis process did not affect the final morphology and size of PLNPs. ZGO-Pt nanoparticles are colloidally stable and monodispersed with a narrow hydrodynamic size distribution (Fig. S2). Moreover, the obtained ZGO-Pt gave a highly crystalline typical cubic spinel structure of $ZnGa_2O_4$ (JCPDS 38–1240), and displayed clear resolved lattice fringes corresponding to the 311 spacing of cubic spinel (Fig. 1B,D). The element Pt in ZGO-Pt was proved by energy dispersive spectroscopy (Fig. 1E). ZGO-Pt gave a bright NIR luminescence emission at ~700 nm (Fig. 1F), originating from the spin forbidden ^2E–$^4A_2$ transition of the distorted Cr^{3+} ions [31–33], as well as an excitation spectrum from 200 nm to 300 nm (Fig. S3). It is noteworthy that ZGO-Pt exhibited stronger NIR emission (700 nm) than original ZGO PLNPs mainly due to the improvement of luminescence efficiency from noble-metal based plasmon enhancement effect [34,35]. Besides, ZGO-Pt showed excellent long-lasting PL features as ZGO, with the PL signal lasted more than 1000 s after 5-min UV light irradiation (254 nm) (Fig. 1G). The above results clearly show that the addition of Pt nanoflower in the synthesis process of ZGO had no adverse impact on the morphology, size, crystal structure and optical performance of ZGO PLNPs.

3.2. Peroxidase mimicking activity of ZGO-Pt

The oxidation reactions of different chromotropic substrates (TMB, ABTS and OPD) with H_2O_2 in the presence of ZGO-Pt were examined to further reveal the catalysis performance of ZGO-Pt. The oxidized products of TMB, ABTS and OPD by H_2O_2 in the presence of ZGO-Pt gave characteristic absorption peaks at 652, 415 and 447 nm, respectively (Fig. 2A), leading to the change of solution color (Fig. S4). In contrast, none of the control groups (in the absence of H_2O_2 or ZGO-Pt) showed these absorption peaks and color change, confirming the inherent peroxide-mimicking enzyme activity of ZGO-Pt nanozyme. Moreover, the peroxide-mimicking enzyme activity of ZGO-Pt depends on the amount of Pt nanoflower added for ZGO-Pt synthesis. The reaction solution of TMB and H_2O_2 showed a negligible absorbance at 652 nm in

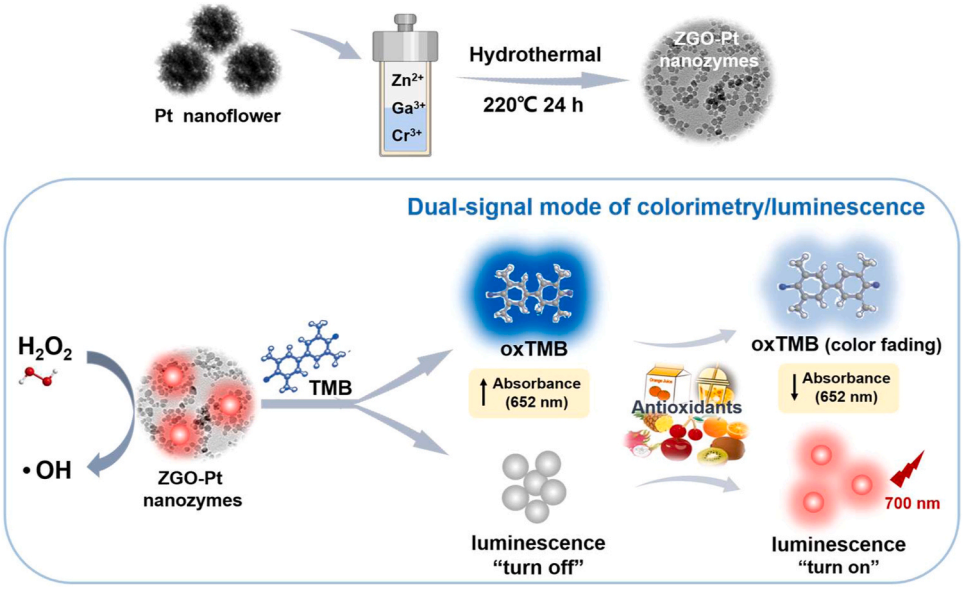

Scheme 1. Schematic illustration of the synthetic procedure of ZGO-Pt and its application for luminescence-colorimetric dual-mode sensing of TAC.

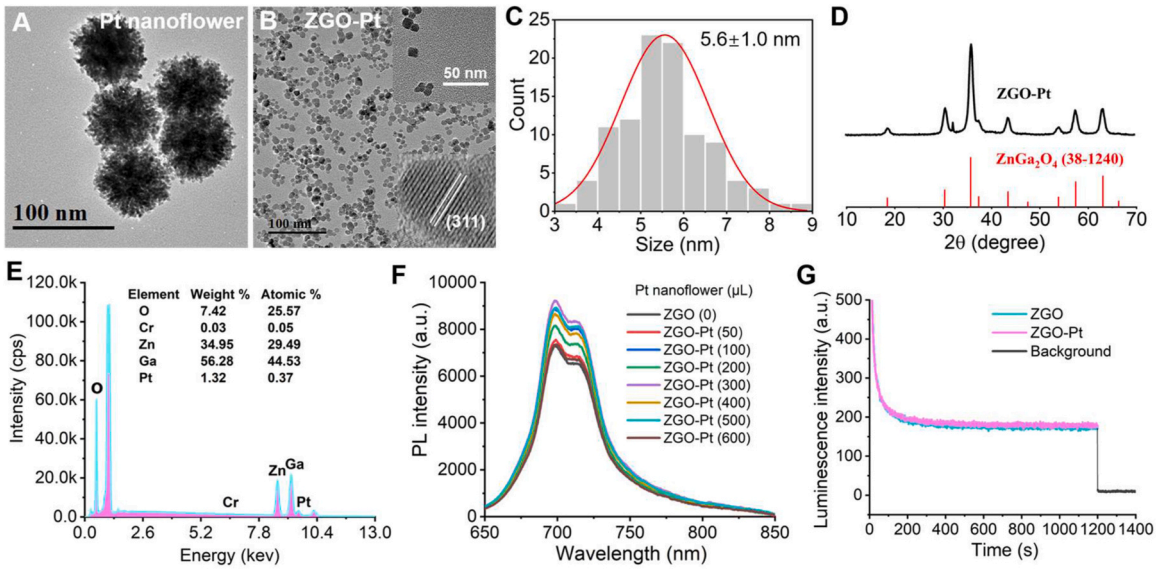

Fig. 1. Characterization of ZGO-Pt nanozymes. TEM images: (A) Pt nanoflower; (B) ZGO-Pt. (C) Size distribution of ZGO-Pt based on 100 randomly selected nanoparticles. (D) XRD pattern and (E) EDS spectrum of ZGO-Pt. (F) PL emission spectra of ZGO-Pt synthesized using various amounts of Pt nanoflower. Ex. 254 nm. (G) Afterglow decay curves of ZGO and ZGO-Pt after 254 nm UV irradiation for 5 min (monitoring emission at 700 nm).

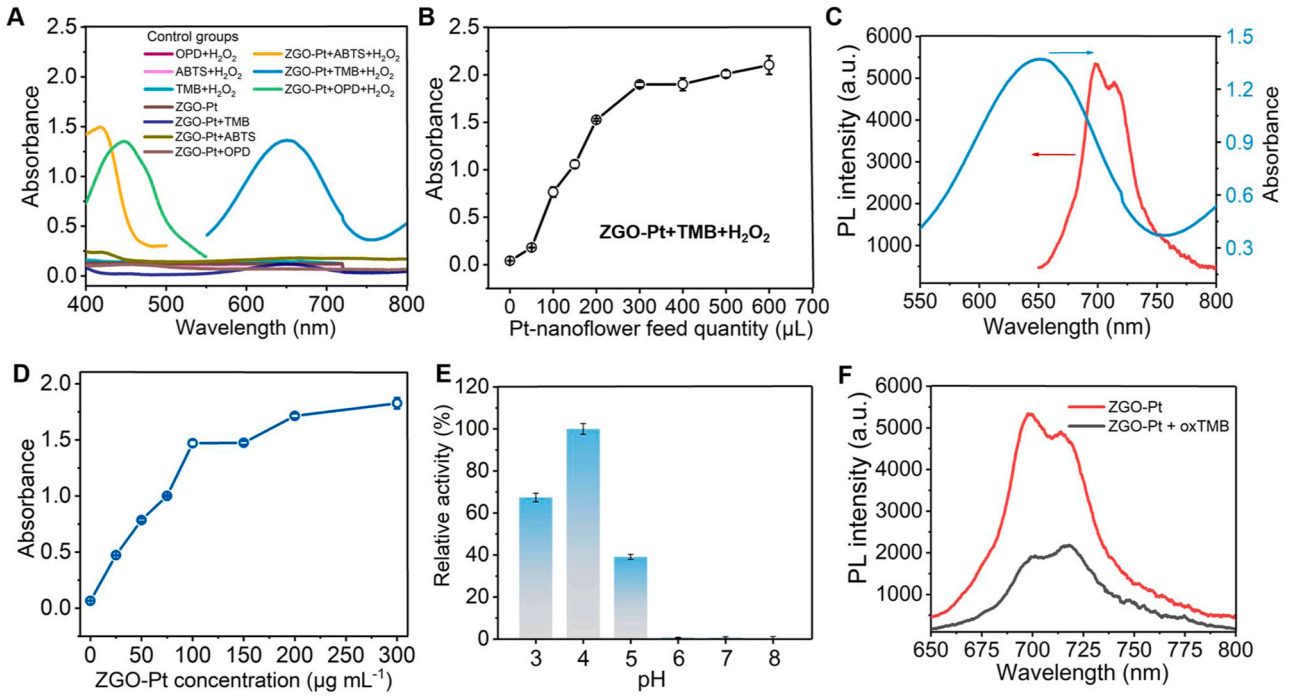

Fig. 2. Peroxidase Mimicking Activity of ZGO-Pt. (A) Absorption spectra of the oxidized products of TMB, ABTS and OPD by H_2O_2 in the presence of ZGO-Pt (TMB, ABTS, OPD (10 μL, 40 mM), H_2O_2 (10 μL, 800 mM). (B) Dependence of the peroxide-mimicking enzyme activity of ZGO-Pt on the feeding amount of Pt nanoflower (TMB (10 μL, 40 mM), H_2O_2 (10 μL, 800 mM) and ZGO-Pt (15 μL, 4 mg mL^{-1})). (C) Luminescence spectrum of the as-prepared ZGO-Pt (120 μg mL^{-1}) and the absorption spectrum of the oxTMB generated under the reaction conditions for (A). (D) Change of the absorbance of the oxidized products of TMB by H_2O_2 with the concentration of ZGO-Pt. (E) Effect of the buffer pH on the peroxidase-mimicking enzyme activity of ZGO-Pt. (F) Change in the PL signal after the oxTMB generation in the presence of ZGO-Pt (TMB (10 μL, 40 mM), H_2O_2 (10 μL, 800 mM) and ZGO-Pt (15 μL, 4 mg mL^{-1}). The reaction solution in (A), (B) and (F) was made up to 400 μL with acetate buffer solution (pH 4.0, 25 mM).

the presence of ZGO (i.e. no addition of Pt nanoflower, 0 μL in Fig. 2B). In contrast, the reaction solution of TMB and H_2O_2 showed a gradual increased absorbance and color change in the presence of ZGO-Pt as the amount of Pt nanoflower added for ZGO-Pt synthesis increased to 300 μL, then no further change in absorbance and color over 300 μL (Fig. 2B and Fig. S5). The above results indicate that the ZGO-Pt prepared with the addition of 300 μL Pt-nanoflower gave the maximum peroxidase-like activity. The comparison of the peroxidase-like activity of the ZGO, Pt nanoflowers and ZGO-Pt further proved that Pt nanoflowers (as synthetic additive) gave ZGO-Pt excellent peroxidase-like activity (Fig. S6). Meanwhile, TMB was chosen as the chromogenic substrate because the absorption spectra of its oxidized

product (oxTMB) overlap the emission spectra of ZGO-Pt for effective quenching of the luminescence of ZGO-Pt (Fig. 2C).

3.3. Optimization of assay parameters

Several working parameters including ZGO-Pt concentration, reaction time, pH and temperature were optimized to clarify the key factors for oxidation reaction to achieve the best peroxidase-like activity. The peroxidase-like activity of the ZGO-Pt was concentration dependent within 120 μg mL^{-1}, then reached a plateau over 120 μg mL^{-1} (Fig. 2D). As depicted in Fig. 2E, the ZGO-Pt exhibited the maximum catalytic activity at pH 4.0 (acetate buffer solution) toward TMB. Consequently, pH 4.0 was used in the following experiments. Fig. S7 reveals that ZGO-Pt kept excellent catalytic activity in a temperature range from 20 °C to 50 °C, and gave the maximum catalytic activity at 35 ℃. Moreover, the reaction equilibrium of the system was reached at 40 min (Fig. S8). Importantly, The PL intensity of the ZGO-Pt was quenched significantly after the oxidation of TMB to oxTMB in reaction system, allowing a huge space for the subsequent responsive "turn on" luminescence sensing (Fig. 2F). As a result, the subsequent studies were carried out with TMB (10 μL, 40 mM), H_2O_2 (10 μL, 800 mM) and ZGO-Pt (120 μg mL^{-1}) at 35 °C for 40 min

3.4. Steady-state kinetic study

Under aforementioned optimal assay conditions, the steady-state kinetic assays were further explored to investigate the affinity of ZGO-Pt towards TMB and H_2O_2 (Supporting Information). Michaelis constant (K_m) and the maximum initial velocity (V_{max}) were calculated according to the Lineweaver-Burk Plots (Fig. 3). K_m is a vital parameter for assessing the affinity of enzymes for substrates, and smaller K_m value indicates greater affinity. As shown in Table S1, the affinity of the as-prepared ZGO-Pt NPs to H_2O_2 and TMB (H_2O_2: 3.12 mM, TMB: 0.592 mM) is comparable to that of horseradish peroxidase (HRP) (H_2O_2: 3.70 mM, TMB: 0.434 mM), indicating its excellent peroxide-mimicking enzyme catalytic efficiency. In addition, ZGO-Pt nanozyme showed negligible reduction in peroxidase activity after ten-cycles use, indicative of its good stability and reusability (Fig. S9).

Catalytic intermediates were further studied to understand the catalytic mechanism by using terephthalic acid (TA) and hydroethidine (HE) as the indicators for •OH and $•O_2^-$ radicals, respectively. Only the system containing TA, H_2O_2 and ZGO-Pt gave high fluorescence intensity of 2-hydroxyterephthalic acid (oxidation products of TA), indicating the production of •OH from H_2O_2 by ZGO-Pt (Fig. S10A). The mechanism of ZGO-Pt catalyzed TMB oxidation in the presence of H_2O_2 is illustrated in Fig. S10B. Moreover, isopropyl alcohol (IPA) was used as the •OH scavengers to further confirm that •OH was the main intermediate responsible for the peroxidase-like activity of ZGO-Pt. The inhibition in TMB/H_2O_2/ZGO-Pt system significantly increased with the introduction of IPA (Fig. S10C). On the other hand, no obvious production of $•O_2^-$was captured in the catalytic process (Fig. S10D,E), indicating that •OH is the primary reactive species in the proposed peroxidase-like enzymatic assay.

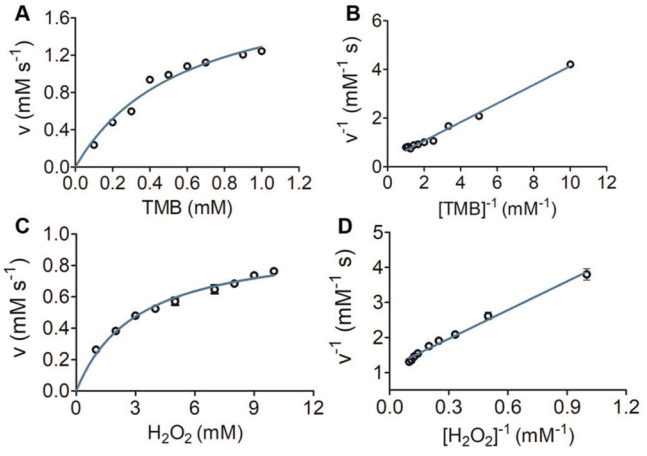

Fig. 3. Steady-state kinetics assays of ZGO-Pt by varying the concentration of (A) TMB (40 mM H_2O_2, ZGO-Pt (100 μg mL^{-1}) and (C) H_2O_2 (1 mM TMB, ZGO-Pt (100 μg mL^{-1})). Lineweaver-Burk plots of ZGO-Pt for (B) TMB and (D) H_2O_2.

3.5. Analytical performance of the developed dual-mode sensor

Ascorbic acid (AA), a typical and common antioxidant, was selected to demonstrate the analytical performance of the developed dual-mode sensor. In colorimetric mode, the absorbance of oxTMB at 652 nm declined with the increase of AA concentration (Fig. 4 A). A linear plot of absorbance change $(A_0\text{-}A)/A_0$ (where A and A_0 are the absorbance in the presence and absence of AA, respectively) against AA concentration was obtained with a determination coefficient R^2 of 0.9969 in the concentration range of 0.5–200 μM (Fig. 4B). The limit of detection (LOD) (3 s) was 0.05 μM and the relative standard deviation (RSD) for 11 replicate determinations of 100 μM AA was 2.7%. Meanwhile, in luminescence mode, the PL intensity in reaction solution increased with AA concentration (Fig. 4 C). A linear plot of the change of PL intensity (ΔPL: $PL\text{-}PL_0$) at 700 nm against AA concentration was obtained with R^2 of 0.9913 from 1 μM to 300 μM (Fig. 4D). The LOD (3 s) was 0.78 μM, and the RSD for 11 replicate determinations of 100 μM AA was 3.8%. In comparison with previous nanomase sensors for AA assay, the fabricated sensor gave wider detection range and lower LOD (Table S2).

3.6. Selectivity of the developed dual-mode sensor

Interferents that may be found in food and food extracts, such as sugars (lactose, saccharose, maltose, galactose, glucose, fructose), common cations (Mg^{2+}, Ca^{2+}, K^+, Na^+), amino acids (histidine, alanine, methionine, tyrosine, proline), urea and five common antioxidants (citric acid, glutathione, oxalic acid, pyrogallic acid and tartaric acid) were selected to study the selectivity of the developed sensor. An obvious change of $(A_0\text{-}A)/A_0$ and persistent luminescence recovery (ΔPL) was observed only in the presence of AA and five antioxidants (Fig. 4E,F), revealing that the addition of interfering chemicals other than antioxidants has little effect on the selectivity of the developed sensor. Among the studied antioxidants, pyrogallic acid demonstrated the highest antioxidant activity, followed by AA. The above results demonstrate that the proposed dual-mode sensor possessed high specificity for the determination of antioxidants and great potential for measuring the total antioxidant capacity of real samples.

3.7. Method validation and application to real sample analysis

TAC usually expressed as AA equivalent antioxidant capacity (micromolar/millimole equivalents of AA). The developed dual-mode sensor was firstly applied for the determination of TAC in a vitamin C tablet. The determined TAC in the vitamin C tablet is in good agreement with the specified content (Fig. 5). The developed sensor was further used to determine TAC in three vitamin C fortified type of compound drinks and three fruits (kiwi, lemon and tomato). The analytical results for these real samples are given in Table 1. It is clear that kiwi gave the highest antioxidant content among three tested fruits, which is conducive to the planning of exogenous dietary antioxidant in daily diet. The determined TAC in these real samples by the developed dual-mode sensor are consistent with those determined by a classical DPPH method (Table 1, Fig. S11). In addition, the recoveries for AA in the tested fruits ranged from 95.4%– 107.6% (Table S3). The above results demonstrate the reliability of our developed dual-mode sensor for the determination of TAC in real sample.

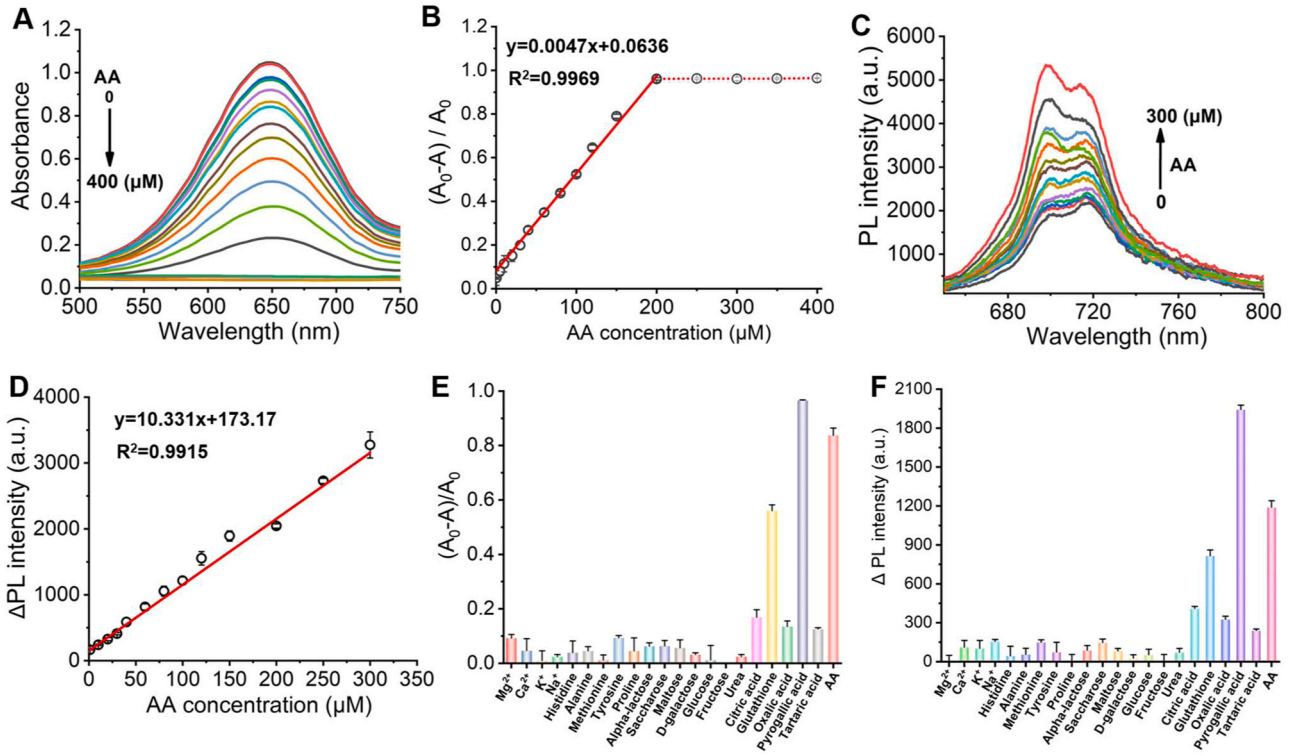

Fig. 4. (A) Change of UV–vis absorption spectrum with AA concentration in the mixture of ZGO-Pt+TMB+H_2O_2 solution. (B) Plot of absorbance change $(A_0\text{-}A)/A_0$ at 652 nm against AA concentration. (C) Change of PL signal with AA concentration in the mixture of ZGO-Pt+TMB+H_2O_2 solution. (D) Plot of ΔPL intensity against AA concentration in the mixture of ZGO-Pt+TMB+H_2O_2 solution. Selectivity of the assay for AA compared to other interferences substances: (E) colorimetry; (F) luminescence. The concentrations of AA and the studied interferents are 100 μM.

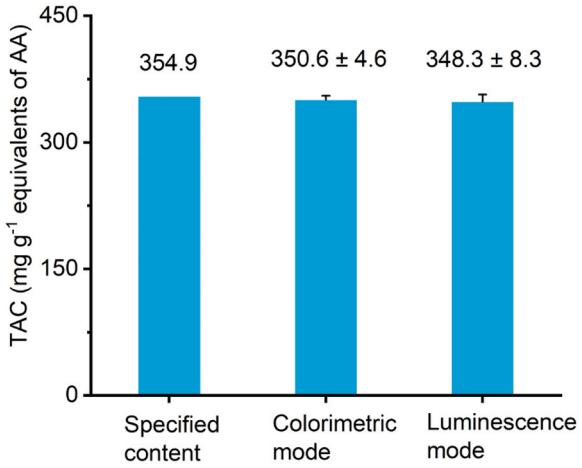

Fig. 5. Comparison of the TAC in a vitamin C tablet determined by the developed ZGO-Pt based dual-mode sensor with the specified value by manufacturer.

4. Conclusion

We have reported a persistent luminescent ZGO-Pt nanozymes-based luminescence-colorimetric dual-mode sensor for selective determination of TAC. The prepared ZGO-Pt integrates the merit of autofluorescence-free persistent luminescence and the excellent catalytic activity for peroxidase mimicking. The highly efficient catalysis of ZGO-Pt allows the dual-mode sensor to realize precise determination of TAC with a wide linear range, low limit of detection and good precision. The dual-mode sensor has been successfully applied to the determination of TAC in vitamin tablet, beverages and fresh fruits. This work not only presents a facile and effective dual-signal mode strategy for TAC evaluation, but also opens the channel between persistent luminescence nanoparticles and nanozymes.

Table 1
Analytical results for determination of TAC in compound drinks and fruit samples.

Sample	Detected equivalents of AA (drinks, mM; fruits, mmol kg^{-1}; mean ± s, n = 3)		
	Colorimetric mode	Luminescence mode	DPPH kit
Drink 1	2.47 ± 0.02	2.49 ± 0.06	2.57 ± 0.04
Drink 2	10.2 ± 0.2	9.72 ± 0.39	9.68 ± 0.32
Drink 3	1.81 ± 0.02	1.91 ± 0.09	1.74 ± 0.08
Tomato	0.377 ± 0.021	0.401 ± 0.035	0.418 ± 0.031
Kiwi	2.06 ± 0.03	2.07 ± 0.03	2.03 ± 0.03
Lemon	0.883 ± 0.063	0.847 ± 0.051	0.835 ± 0.016

CRediT authorship contribution statement

Yan Li-Xia: Conceptualization, Data curation, Investigation, Methodology, Writing – original draft. **Yan Zhu-Ying:** Investigation, Methodology. **Zhao Xu:** Methodology, Writing – review & editing. **Chen Li-Jian:** Methodology, Writing – review & editing. **Yan Xiu-Ping:** Conceptualization, Funding acquisition, Supervision, Writing – review & editing.

Declaration of Competing Interest

The authors declare that they have no known competing financial interests or personal relationships that could have appeared to influence the work reported in this paper.

Data Availability

Data will be made available on request.

Acknowledgements

This work was supported by the National Natural Science Foundation of China (No. 21934002, 22206060, and 22304063), the Natural Science Foundation of Jiangsu Province, China (No. BK20231033).

Appendix A. Supporting information

Supplementary data associated with this article can be found in the online version at doi:10.1016/j.snb.2024.135333.

References

[1] J. Li, Y. Zhou, Y. Xiao, S. Cai, C. Huang, S. Guo, Y. Sun, R.-B. Song, Z. Li, Carbon dots as light-responsive oxidase-like nanozyme for colorimetric detection of total antioxidant capacity in fruits, Food Chem. 405 (2023) 134749, https://doi.org/10.1016/j.foodchem.2022.134749.

[2] L.U. Pagan, M.J. Gomes, M. Gatto, G.A. Mota, K. Okoshi, M.P. Okoshi, The role of oxidative stress in the aging heart, Antioxidants 11 (2022) 336, https://doi.org/10.3390/antiox11020336.

[3] J.M. Lorenzo, P.E.S. Munekata, B. Gómez, F.J. Barba, L. Mora, C. Pérez-Santaescolástica, F. Toldrá, Bioactive peptides as natural antioxidants in food products–a review, Trends Food Sci. Technol. 79 (2018) 136–147, https://doi.org/10.1016/j.tifs.2018.07.003.

[4] N. Yaghoubi, M. Youssefi, F. Jabbari Azad, F. Farzad, Z. Yavari, F. Zahedi Avval, Total antioxidant capacity as a marker of severity of COVID-19 infection: Possible prognostic and therapeutic clinical application, J. Med. Virol. 94 (2022) 1558–1565, https://doi.org/10.1002/jmv.27500.

[5] H.J. Forman, H. Zhang, Targetting oxidative stress in disease: promise and limitations of antioxidant therapy, Nat. Rev. Drug Discov. 20 (2021) 689–709, https://doi.org/10.1038/s41573-021-00233-1.

[6] W. Wang, P.M. Kang, Oxidative stress and antioxidant treatments in cardiovascular diseases, Antioxidant 9 (2020) 1292, https://doi.org/10.3390/antiox9121292.

[7] L.-T. Sheng, Y.-W. Jiang, L. Feng, A. Pan, W.-P. Koh, Dietary total antioxidant capacity and late-life cognitive impairment: the singapore chinese health study, J. Gerontol. A. 77 (2022) 561–569, https://doi.org/10.1093/gerona/glab100.

[8] A. Jayedi, A. Rashidy-Pour, M. Parohan, M.S. Zargar, S. Shab-Bidar, Dietary antioxidants, circulating antioxidant concentrations, total antioxidant capacity, and risk of all-cause mortality: a systematic review and dose-response meta-analysis of prospective observational studies, Adv. Nutr. 9 (2018) 701–716, https://doi.org/10.1093/advances/nmy040.

[9] R. Szymanska, P. Pospíšil, J. Kruk, Plant-derived antioxidants in disease prevention 2018, Oxid. Med. Cell. Longev. (2018) 2068370, https://doi.org/10.1155/2018/2068370.

[10] M. Serafini, R. Bellocco, A. Wolk, A.M. Ekström, Total antioxidant potential of fruit and vegetables and risk of gastric cancer, Gastroenterology 123 (2002) 985–991, https://doi.org/10.1053/gast.2002.35957.

[11] L. Fu, B.-T. Xu, X.-R. Xu, R.-Y. Gan, Y. Zhang, E.-Q. Xia, H.-B. Li, Antioxidant capacities and total phenolic contents of 62 fruits, Food Chem. 129 (2011) 345–350, https://doi.org/10.1016/j.foodchem.2011.04.079.

[12] N. Song, Y. Zhang, S. Ren, C. Wang, X. Lu, Rational design of conducting polymer-derived tubular carbon nanoreactors for enhanced enzyme-like catalysis and total antioxidant capacity bioassay application, Anal. Chem. 94 (2022) 11695–11702, https://doi.org/10.1021/acs.analchem.2c02511.

[13] X. Han, L. Liu, H. Gong, L. Luo, Y. Han, J. Fan, C. Xu, T. Yue, J. Wang, W. Zhang, Dextran-stabilized Fe-Mn bimetallic oxidase-like nanozyme for total antioxidant capacity assay of fruit and vegetable food, Food Chem. 371 (2022) 131115, https://doi.org/10.1016/j.foodchem.2021.131115.

[14] Q. Hu, H. Sun, X. Zhou, X. Gong, L. Xiao, L. Liu, Z.-Q. Yang, Bright-yellow-emissive nitrogen-doped carbon nanodots as a fluorescent nanoprobe for the straightforward detection of glutathione in food samples, Food Chem. 325 (2020) 126946, https://doi.org/10.1016/j.foodchem.2020.126946.

[15] Q. Jiao, W. Zhang, Y. Jiang, L. Jiang, X. Chen, B. Liu, Study on the interactions between caffeoylquinic acids with bovine serum albumin: spectroscopy, antioxidant activity, lc-msn, and molecular docking approach, Front. Chem. 7 (2019) 840, https://doi.org/10.3389/fchem.2019.00840.

[16] Y. Zheng, X. Li, C. Wei, Y. Gao, G. Han, J. Zhao, C. Zhang, K. Zhang, Z. Zhang, Long-lived phosphorescent carbon dots as photosensitizers for total antioxidant capacity assay, Anal. Chem. 95 (2023) 8914–8921, https://doi.org/10.1021/acs.analchem.3c00657.

[17] I.G. Munteanu, C. Apetrei, Analytical methods used in determining antioxidant activity: a review, Int. J. Mol. Sci. 22 (2021) 3380, https://doi.org/10.3390/ijms22073380.

[18] Y.-W. Mao, J.-Q. Li, R. Zhang, A.-J. Wang, J.-J. Feng, Nitrogen-doped carbon nanoflowers decorated with PtNi nanoparticles for colorimetric detection of total antioxidant capacity, ACS Appl. Nano Mater. 6 (2023) 2805–2812, https://doi.org/10.1021/acsanm.2c05199.

[19] J. Zeng, Y. Zhang, T. Zeng, R. Aleisa, Z. Qiu, Y. Chen, J. Huang, D. Wang, Z. Yan, Y. Yin, Anisotropic plasmonic nanostructures for colorimetric sensing, Nano Today 32 (2020) 100855, https://doi.org/10.1016/j.nantod.2020.100855.

[20] S. Li, P. Keoingthong, J. Xu, Y. Yang, J. Shen, Y. Xu, L. Zhang, X. Xia, X. Cao, S. Wang, Z. Chen, Highly efficient carbon supported Co-Ir nanozyme for the determination of total antioxidant capacity in foods, Biosens. Bioelectron. 236 (2023) 115416, https://doi.org/10.1016/j.bios.2023.115416.

[21] Y. Li, R. Javed, R. Li, Y. Zhang, Z. Lang, H. Zhao, X. Liu, H. Cao, D. Ye, A colorimetric smartphone-based sensor for on-site AA detection in tropical fruits using Fe-P/NC single-atom nanoenzyme, Food Chem. 406 (2023) 135017, https://doi.org/10.1016/j.foodchem.2022.135017.

[22] W. Liu, L. Chu, C. Zhang, P. Ni, Y. Jiang, B. Wang, Y. Lu, C. Chen, Hemin-assisted synthesis of peroxidase-like Fe-N-C nanozymes for detection of ascorbic acid-generating bio-enzymes, Chem. Eng. J. 415 (2021) 128876, https://doi.org/10.1016/j.cej.2021.128876.

[23] T. Wang, J. Feng, H. Sun, Y. Liang, T. Du, J. Dan, J. Wang, W. Zhang, CuBi bimetallic aerogel as peroxidase-like nanozyme for total antioxidant capacity colorimetric detection, Sens. Actuators B: Chem. 379 (2023) 133249, https://doi.org/10.1016/j.snb.2022.133249.

[24] C. Hong, L. Chen, J. Huang, Y. Shen, H. Yang, Z. Huang, R. Cai, W. Tan, Gold nanoparticle-decorated MoSe2 nanosheets as highly effective peroxidase-like nanozymes for total antioxidant capacity assay, Nano Res 16 (2023) 7180–7186, https://doi.org/10.1007/s12274-022-5328-9.

[25] Y. Zhang, Y.-S. Feng, X.-H. Ren, X.-W. He, W.-Y. Li, Y.-K. Zhang, Bimetallic molecularly imprinted nanozyme: Dual-mode detection platform, Biosens. Bioelectron. 196 (2022) 113718, https://doi.org/10.1016/j.bios.2021.113718.

[26] B.-B. Wang, X. Zhao, L.-J. Chen, C. Yang, X.-P. Yan, Functionalized persistent luminescence nanoparticle-based aptasensor for autofluorescence-free determination of kanamycin in food samples, Anal. Chem. 93 (2021) 2589–2595, https://doi.org/10.1021/acs.analchem.0c04648.

[27] L.-M. Pan, X. Zhao, X. Wei, L.-J. Chen, C. Wang, X.-P. Yan, Ratiometric luminescence aptasensor based on dual-emissive persistent luminescent nanoparticles for autofluorescence- and exogenous interference-free determination of trace aflatoxin B1 in food samples, Anal. Chem. 94 (2022) 6387–6393, https://doi.org/10.1021/acs.analchem.2c00861.

[28] B.-Y. Wu, H.-F. Wang, J.-T. Chen, X.-P. Yan, Fluorescence resonance energy transfer inhibition assay for α-fetoprotein excreted during cancer cell growth using functionalized persistent luminescence nanoparticles, J. Am. Chem. Soc. 133 (2011) 686–688, https://doi.org/10.1021/ja108788p.

[29] K. Chen, X. Peng, M. Dang, J. Tao, J. Ma, Z. Li, L. Zheng, X. Su, L. Wang, Z. Teng, General thermodynamic-controlled coating method to prepare janus mesoporous nanomotors for improving tumor penetration, ACS Appl. Mater. Interfaces 13 (2021) 51297–51311, https://doi.org/10.1021/acsami.1c11838.

[30] B. Fu, M. Dang, J. Tao, Y. Li, Y. Tang, Mesoporous platinum nanoparticle-based nanoplatforms for combined chemo-photothermal breast cancer therapy, J. Colloid Interface Sci. 570 (2020) 197–204, https://doi.org/10.1016/j.jcis.2020.02.051.

[31] Z. Pan, Y.-Y. Lu, F. Liu, Sunlight-activated long-persistent luminescence in the near-infrared from Cr^{3+}-doped zinc gallogermanates, Nat. Mater. 11 (2012) 58–63, https://doi.org/10.1038/nmat3173.

[32] Y. Wang, C.-X. Yang, X.-P. Yan, Hydrothermal and biomineralization synthesis of a dual-modal nanoprobe for targeted near-infrared persistent luminescence and magnetic resonance imaging, Nanoscale 9 (2017) 9049–9055, https://doi.org/10.1039/C7NR02038D.

[33] A. l. Bessière, S.K. Sharma, N. Basavaraju, K.R. Priolkar, L. Binet, B. Viana, A.J. Bos, T. Maldiney, C. Richard, D. Scherman, Storage of visible light for long-lasting phosphorescence in chromium-doped zinc gallate, Chem. Mater. 26 (2014) 1365–1373, https://doi.org/10.1021/cm403050q.

[34] J.-M. Liu, Y.-Y. Liu, D.-D. Zhang, G.-Z. Fang, S. Wang, Synthesis of $GdAlO_3$: Mn^{4+}, Ge^{4+}@Au COre–shell Nanoprobes with Plasmon-enhanced Near-infrared Persistent Luminescence for in Vivo Tri-modality Bioimaging, ACS Appl. Mater. Interfaces 8 (2016) 29939–29949, https://doi.org/10.1021/acsami.6b09580.

[35] L. Liang, J. Chen, K. Shao, X. Qin, Z. Pan, X. Liu, Controlling persistent luminescence in nanocrystalline phosphors, Nat. Mater. 22 (2023) 289–304, https://doi.org/10.1038/s41563-022-01468-y.

Li-Xia Yan is a postdoctoral research associate at Jiangnan University, China. Her research interest includes advanced functional materials for bioanalysis and bioimaging.

Zhu-Ying Yan is a technician at Jiangnan University, China.

Xu Zhao is an associate professor at Jiangnan University, China. Her research interest includes advanced materials for analytical chemistry and food safety.

Li-Jian Chen is an associate professor at Jiangnan University, China. Her research interest includes advanced materials for analytical chemistry and food safety.

Xiu-Ping Yan is the Cheung Kong Distinguished Professor at Jiangnan University, China. He is the editor for Analytica Chimica Acta, associate editor for Frontier in Environmental Science, and he is also the member of the editorial (advisory) board for Talanta, Electrophoresis, and Cancer Nanotechnology. His research interests include hyphenated techniques and advanced functional materials for food and environmental analysis, bioanalysis, and bioimaging.